

Geometrically Nonlinear Analysis of Functionally Graded Shells Based on 2-D Cosserat Constitutive Model

Karol DASZKIEWICZ, Jacek CHRÓŚCIELEWSKI, Wojciech WITKOWSKI

Gdańsk University of Technology
Faculty of Civil and Environmental Engineering
Department of Structural Mechanics
Narutowicza 11/12, 80-233 Gdańsk, Poland
e-mail: kardasz@pg.gda.pl

In this paper geometrically nonlinear analysis of functionally graded shells in 6-parameter shell theory is presented. It is assumed that the shell consists of two constituents: ceramic and metal. The mechanical properties are graded through the thickness and are described by power law distribution. Formulation based on 2-D Cosserat constitutive model is used to derive constitutive relation for functionally graded shells. Numerical results for typical benchmark geometries of smooth and irregular FGM shells under mechanical loading are presented. The influence of power-law exponent and micropolar material constants on the overall behaviour of functionally graded shells is investigated.

Key words: functionally graded shells, nonlinear six-parameter shell theory, Cosserat constitutive equations, micropolar constants, large deflection.

1. INTRODUCTION

The material known as “functionally graded material” (FGM), was probably first proposed in 1984 by a group of material scientists in Japan [1]. Continuous changes in the composition of constituent materials, microstructure, porosity of the FGM material result in gradients of material properties. Functionally graded shells are usually made from ceramic and metal. The connection of these materials gives high heat-resistance and high mechanical strength shells. The volume fraction of ceramic and metal is varying through the thickness of the shell from one surface to the other. In laminated composite structures discontinuous change of the material properties at interface surface sometimes leads to delamination failure due to sliding and cracking. FGM shells do not have this material mismatch because continuous and smooth change in the material properties eliminates discrete changes in the stress and displacement distributions. Furthermore, there is possibility to design a functionally graded shell for

specific application by choosing an appropriate type of materials, shell thickness and material distribution.

With increasing application of FGM shells, it is important to investigate the behaviour of shells in nonlinear range. Many geometrically nonlinear studies have been performed for isotropic and laminated composite shells, see e.g. [2]. However, a review of literature shows that only the limited number of studies have been carried out to analyze the nonlinear response of FGM plates and shells. The results of nonlinear analysis of simply supported square functionally graded plate under transverse mechanical load have been presented in [3] and for immovable hinged edges in [4]. The closed-form analytical solutions for rectangular plates [5], illustrated by the Fourier series expansion, were compared with the finite element solutions in [6]. Large deflection and postbuckling analysis of functionally graded rectangular plates under transverse and in-plane loads using a semi-analytical approach have been performed in [7] and for circular plates subjected to mechanical and thermal load in [8]. Numerical results obtained using higher-order elements for typical benchmark problem geometries of FGM regular shells have been presented in [9]. In book [10] nonlinear response of functionally graded shells and plates to nonlinear bending, postbuckling and nonlinear vibration has been investigated. An example of dynamic buckling analysis of thin FGM plate has been presented in [11] and nonlinear bending analysis of FGM rectangular plates on two-parameter elastic foundations in [12].

In this paper, a geometrically nonlinear FEM analysis of FGM shells is presented. The formulation is based on the nonlinear 6-parameter shell theory [13], where the sixth parameter is drilling degree of freedom. The kinematic model, formally equivalent to the Cosserat surface, is obtained from through-the-thickness integration of 3D balance laws of linear and angular momentum of the Cauchy continuum. The foundations of the theory of asymmetric elasticity were laid down by Cosserat brothers [14]. An extensive historical study about the materials with internal structure may be found, for instance in [15–17]. Some constitutive relations for elastic isotropic shells with drilling degree of freedom have been presented in [13, 18–21] and for composite shells in [22]. Recently the elastoplastic material law obtained by the Reissner-Mindlin type through-the-thickness integration of the plane stress Cosserat relation has been proposed in [23, 24].

In comparison with [3–12] where the Cauchy continuum is used, here we use the formulation based on 2-D Cosserat constitutive model to describe kinematic of functionally graded shells. Early results we have presented for simply supported square plate in [25] and for pinched cylinder with free edges in [26]. The constitutive relation is based on the assumptions: first order shear deformation theory (FOSD, e.g. [27] or Reissner-Mindlin kinematics), small strains, finite displacements and rotations. The closed-form of constitutive matrix is obtained by

through-the-thickness integration of the plane stress Cosserat material law. We assume the shell base surface as geometrical middle surface. Numerical results are presented for typical benchmark geometries of thin, smooth and irregular FGM shells. We also investigate the influence of micropolar material parameters on the overall behaviour of functionally graded shells. A similar approach can be found in [28], yet different shell kinematic is used there in comparison to this paper.

2. FUNCTIONALLY GRADED SHELLS

Functionally graded materials (FGMs) are microscopically inhomogeneous composites in which the material properties exhibit continuous and smooth change from one surface to another. This characteristic allows for eliminating interface problems and mitigate thermal stress concentrations. In this paper, we analyze the most popular in the literature [3–12] case of functionally graded shell which top surface is ceramic-rich and bottom surface is metal-rich (Fig. 1).

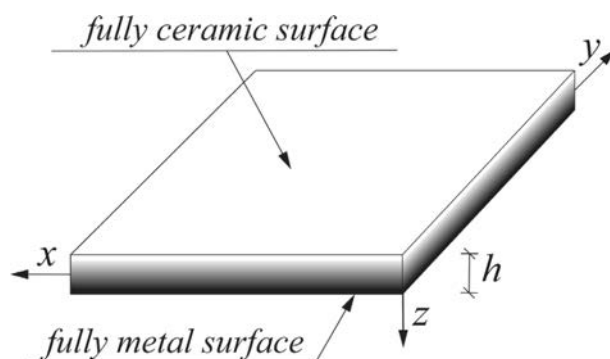


FIG. 1. Typical functionally graded shell.

The effective material properties $P(z)$ (for instance Young's modulus) in the lamina of FGM shell may be calculated by using a simple rule of mixture of constituent material properties P_i , $i = c, m$

$$(2.1) \quad P(z) = P_c V_c + P_m V_m, \quad -\frac{h}{2} \leq z \leq \frac{h}{2},$$

where the subscripts c and m refer to ceramic and metal constituents, V_i is the volume fraction of constituent material i and z is the coordinate in the thickness direction (Fig. 1).

In the literature one may find different functions describing variation of volume fraction of constituent materials through the shell thickness. The results

for power-law, sigmoid and exponential function have been presented, e.g. in [5, 6]. When precise information about distribution of particles is not available, the micromechanical models [10] may be used to obtain effective properties. In this work, we assume that volume fraction distributions of the ceramic V_c and metal V_m are expressed by the power law

$$(2.2) \quad V_c = \left(\frac{z}{h} + \frac{1}{2} \right)^n, \quad V_m = 1 - V_c, \quad n \geq 0,$$

where n is the volume fraction exponent. The shell base surface is defined as geometrical middle surface. For $n = 0$ we obtain a fully ceramic shell, and as n tends to infinity we have a fully metal shell (Fig. 2). Considering (2.1), (2.2) the material properties $P(z)$, like Young's modulus $E(z)$, density $\rho(z)$ and the shear modulus $G(z)$, are functions of the thickness coordinate z

$$(2.3) \quad P(z) = (P_c - P_m) \left(\frac{z}{h} + \frac{1}{2} \right)^n + P_m.$$

Variation of the material properties through the thickness of the shell for different values of exponent n is presented in Fig. 2.

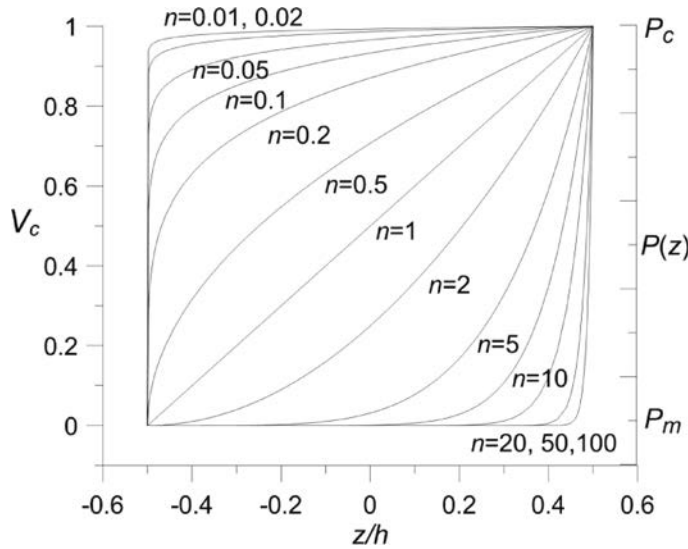


FIG. 2. Variation of the volume fraction of the ceramic and of the material properties through the thickness.

Considering that the effect of changing Poisson's ratio ν in the thickness direction on the results is very small [6], in this work, we assume that the Poisson's ratio is constant in the shell. During determining the components of

constitutive matrix we calculate following integrals of Young's modulus through the thickness:

$$(2.4) \quad E_1 = \frac{1}{h} \int_{-h/2}^{h/2} E(z) dz$$

$$= \frac{1}{h} \int_{-h/2}^{h/2} (E_c - E_m) \left(\frac{z}{h} + \frac{1}{2} \right)^n dz + \frac{1}{h} \int_{-h/2}^{h/2} E_m dz = \frac{E_c - E_m}{n+1} + E_m,$$

$$(2.5) \quad E_2 = \frac{1}{h^2} \int_{-h/2}^{h/2} E(z) z dz = (E_c - E_m) \left[\frac{1}{(n+2)} - \frac{1}{2(n+1)} \right],$$

$$(2.6) \quad E_3 = \frac{12}{h^3} \int_{-h/2}^{h/2} E(z) z^2 dz = (E_c - E_m) \left[\frac{3}{(n+1)} - \frac{12}{(n+2)} + \frac{12}{(n+3)} \right] + E_m.$$

The moduli E_1 , E_2 , E_3 will be used in next section to derive analytical closed-form of constitutive matrix.

Direct analysis of functionally graded shells in FEM commercial programs is not generally available. However user may model FGM shell as a composite shell consisting of many layers. In this method the Young's modulus of composite layers is calculated in the middle of each layer according to (2.3). This approach gives approximated results because distribution of the material properties through the thickness is discrete, and as the number of layers will increase the results will be more precise. This method has been used for instance in [11] and in this paper during calculation in commercial program Abaqus.

3. CONSTITUTIVE RELATION

This section shows derivation of the 2D constitutive relation for functionally graded shell which general form is

$$(3.1) \quad \mathbf{s} = \mathbf{C} \boldsymbol{\varepsilon}.$$

We assemble the strain components on the shell base surface in the one column array (vector form)

$$(3.2) \quad \boldsymbol{\varepsilon} = \{ \varepsilon_{11} \ \varepsilon_{22} \ \varepsilon_{12} \ \varepsilon_{21} \mid \varepsilon_1 \ \varepsilon_2 \mid \kappa_{11} \ \kappa_{22} \ \kappa_{12} \ \kappa_{21} \mid \kappa_1 \ \kappa_2 \}^T = \{ \boldsymbol{\varepsilon}_m \mid \boldsymbol{\varepsilon}_s \mid \boldsymbol{\varepsilon}_b \mid \boldsymbol{\varepsilon}_d \}^T,$$

where letters m, s, b, d denote the following components: the membrane, shear, bending and drilling, respectively. The Cosserat type strain measures on the shell base surface may be written as, see e.g. [13]

$$(3.3) \quad \boldsymbol{\varepsilon}_\beta = \mathbf{y}_{,\beta} - \mathbf{t}_\beta, \quad \delta \boldsymbol{\varepsilon}_\beta = \mathbf{v}_{,\beta} + \mathbf{y}_{,\beta} \times \mathbf{w}, \quad \beta = 1, 2.$$

In the above equation $\mathbf{t}_i(\mathbf{x})$ ($i = 1, 2, 3$) is the orthogonal basis in the current placement of the shell, $\mathbf{v}(\mathbf{x})$ and $\mathbf{w}(\mathbf{x})$ are vector fields of virtual translations and virtual rotations, respectively. Comma in (3.3) and further indicates partial differentiation with respect to the surface coordinates. For the curvatures the following definitions hold, see e.g. [13]

$$(3.4) \quad \boldsymbol{\kappa}_\beta = \text{axl}(\mathbf{Q}_{,\beta} \mathbf{Q}^T), \quad \delta \boldsymbol{\kappa}_\beta = \mathbf{w}_{,\beta}.$$

In (3.4) $\text{axl}(\dots)$ is the operator defining an axial vector of some skew tensor and $\mathbf{Q}(\mathbf{x})$ is an independent proper orthogonal tensor field computed here through canonical parametrization, described, for instance in [29]. The strain components in (3.2) are defined by component form of equations (3.3)₁ and (3.4)₁

$$(3.5) \quad \boldsymbol{\varepsilon}_\beta = \varepsilon_{\beta 1} \mathbf{t}_1 + \varepsilon_{\beta 2} \mathbf{t}_2 + \varepsilon_{\beta 3} \mathbf{t}_3, \quad \boldsymbol{\kappa}_\beta = \mathbf{t}_3 \times (\kappa_{\beta 1} \mathbf{t}_1 + \kappa_{\beta 2} \mathbf{t}_2) + \kappa_{\beta 3} \mathbf{t}_3.$$

Correspondingly to (3.2) we populate one column array of the shell stress and couple resultants

$$(3.6) \quad \mathbf{s} = \{N^{11} N^{22} N^{12} N^{21} | Q^1 Q^2 | | M^{11} M^{22} M^{12} M^{21} | M^1 M^2\}^T = \{\mathbf{s}_m | \mathbf{s}_s | \mathbf{s}_b | \mathbf{s}_d\}^T.$$

The column arrays (3.2) and (3.6) are energy conjugated. Detailed formulation of the 6-parameter shell theory and mathematical background one may found in [13, 18–20] and references given there.

In this paper we use the formulation described recently in works [23–25]. We assume the plane Cosserat stress in each lamina of the shell. Then the one column arrays (vectors) of generalized stresses and strains for lamina of the shell have form

$$(3.7) \quad \mathbf{e} = \begin{Bmatrix} \mathbf{e}_m \\ \dots \\ \mathbf{e}_d \end{Bmatrix} = \begin{Bmatrix} \varepsilon_{11} \\ \varepsilon_{22} \\ \varepsilon_{12} \\ \varepsilon_{21} \\ \dots \\ \varepsilon_1 \\ \varepsilon_2 \end{Bmatrix} = \begin{Bmatrix} \varepsilon_{11} \\ \varepsilon_{22} \\ \varepsilon_{12} \\ \varepsilon_{21} \\ \dots \\ \kappa_1 \cdot l \\ \kappa_2 \cdot l \end{Bmatrix}, \quad \boldsymbol{\sigma} = \begin{Bmatrix} \boldsymbol{\sigma}_m \\ \dots \\ \boldsymbol{\sigma}_d \end{Bmatrix} = \begin{Bmatrix} \sigma_{11} \\ \sigma_{22} \\ \sigma_{12} \\ \sigma_{21} \\ \dots \\ \sigma_1 \\ \sigma_2 \end{Bmatrix} = \begin{Bmatrix} \sigma_{11} \\ \sigma_{22} \\ \sigma_{12} \\ \sigma_{21} \\ \dots \\ m_1/l \\ m_2/l \end{Bmatrix},$$

where l is the micropolar characteristic length – material parameter. Introduction of l in (3.7)_{1,2} gives all the components the same physical dimension.

The elastic constitutive relation of the plane Cosserat stress is following

$$(3.8) \quad \boldsymbol{\sigma} = \mathbf{C}^e \mathbf{e},$$

where \mathbf{C}^e is the constitutive matrix of the shell lamina defined as

$$(3.9) \quad \mathbf{C}^e = \left[\begin{array}{cc|cc} \mathbf{C}_{mm} & \mathbf{C}_{md} \\ \mathbf{C}_{dm} & \mathbf{C}_{dd} \end{array} \right] = \left[\begin{array}{cccc|cc} Ea_1 & Ea_2 & 0 & 0 & 0 & 0 \\ Ea_2 & Ea_1 & 0 & 0 & 0 & 0 \\ 0 & 0 & G + G_c & G - G_c & 0 & 0 \\ 0 & 0 & G - G_c & G + G_c & 0 & 0 \\ \hline 0 & 0 & 0 & 0 & 2G & 0 \\ 0 & 0 & 0 & 0 & 0 & 2G \end{array} \right]$$

$$= \left[\begin{array}{cccc|cc} Ea_1 & Ea_2 & 0 & 0 & 0 & 0 \\ Ea_2 & Ea_1 & 0 & 0 & 0 & 0 \\ 0 & 0 & G\mu_1 & G\mu_2 & 0 & 0 \\ 0 & 0 & G\mu_2 & G\mu_1 & 0 & 0 \\ \hline 0 & 0 & 0 & 0 & 2G & 0 \\ 0 & 0 & 0 & 0 & 0 & 2G \end{array} \right].$$

Here $a_1 = \frac{1}{1 - \nu^2}$, $a_2 = \nu a_1$ and G_c is micropolar modulus [15]. Additionally in further part of section we will use symbols $\mu_1 = \frac{1}{1 - N^2}$ and $\mu_2 = \frac{1 - 2N^2}{1 - N^2}$ in which, following [30], $N^2 = \frac{G_c}{G + G_c}$ is the Cosserat coupling number. In the papers [31, 32] experimental methods for determining the micropolar constitutive parameters for elastic solids are described.

We further employ the kinematical assumption of Mindlin-Reissner, known also as the first order shear deformation (FOSD) theory, e.g. [27]. Paper [33] shows that for thin plates higher-order shear theories and FOSD give almost the same results. One column array (vector form) of the strain components \mathbf{e} in the shell space under FOSD hypothesis follow from known strains $\boldsymbol{\varepsilon}$ (3.2) at the shell base surface as

$$(3.10) \quad \mathbf{e}_m = \boldsymbol{\varepsilon}_m + z \boldsymbol{\varepsilon}_b,$$

where z is the coordinate through the thickness of the shell h which varies from $h^- = -h/2$ to $h^+ = h/2$. For drilling components of strains we propose the following relation

$$(3.11) \quad \mathbf{e}_d = \boldsymbol{\varepsilon}_d \cdot \mathbf{l}.$$

However, recently in paper [34] has been shown that, in some cases, the drilling couples is connected also with membrane strain components.

During calculation of the stress resultants we assume that $\mu \approx 1$ with μ being the determinant of the shifter tensor $\mu_{\alpha\beta}$. This simplification is reasonable only for thin shells with a small curvature $h \ll R_{\min}$. Through the thickness integration of stresses using (3.8)–(3.11) we obtain the membrane, bending and drilling stress resultants (3.6) as functions of the strains defined in (3.2):

$$(3.12) \quad \mathbf{s}_m = \int_{h^-}^{h^+} \boldsymbol{\sigma}_m dz = \int_{h^-}^{h^+} [\mathbf{C}_{mm}(\boldsymbol{\varepsilon}_m + z\boldsymbol{\varepsilon}_b) + \mathbf{C}_{md}l \cdot \boldsymbol{\varepsilon}_d] dz$$

$$= E_1 c \mathbf{H}_{mm} \boldsymbol{\varepsilon}_m + E_2 b \mathbf{H}_{mm} \boldsymbol{\varepsilon}_b,$$

$$(3.13) \quad \mathbf{s}_b = \int_{h^-}^{h^+} \boldsymbol{\sigma}_m z dz = \int_{h^-}^{h^+} [\mathbf{C}_{mm}(z\boldsymbol{\varepsilon}_m + z^2\boldsymbol{\varepsilon}_b) + zl \cdot \mathbf{C}_{md}\boldsymbol{\varepsilon}_d] dz$$

$$= E_2 b \mathbf{H}_{mm} \boldsymbol{\varepsilon}_m + E_3 d \mathbf{H}_{mm} \boldsymbol{\varepsilon}_b,$$

$$(3.14) \quad \mathbf{s}_d = \int_{h^-}^{h^+} l \cdot \boldsymbol{\sigma}_d dz = \int_{h^-}^{h^+} [l \cdot \mathbf{C}_{dm}(\boldsymbol{\varepsilon}_m + z\boldsymbol{\varepsilon}_b) + l^2 \cdot \mathbf{C}_{dd} \cdot \boldsymbol{\varepsilon}_d] dz$$

$$= \int_{h^-}^{h^+} l^2 \cdot \mathbf{C}_{dd} \cdot \boldsymbol{\varepsilon}_d dz = G_1 \mathbf{H}_{dd} \boldsymbol{\varepsilon}_d,$$

where

$$c = \frac{h}{1 - \nu^2}, \quad b = \frac{h^2}{1 - \nu^2}, \quad d = \frac{h^3}{12(1 - \nu^2)},$$

$$G_1 = \frac{E_1}{2(1 + \nu)}$$

and \mathbf{H}_{mm} , \mathbf{H}_{dd} are coefficients matrices

$$(3.15) \quad \mathbf{H}_{mm} = \begin{bmatrix} 1 & \nu & 0 & 0 \\ \nu & 1 & 0 & 0 \\ 0 & 0 & \mu_1(1 - \nu)/2 & \mu_2(1 - \nu)/2 \\ 0 & 0 & \mu_2(1 - \nu)/2 & \mu_1(1 - \nu)/2 \end{bmatrix}, \quad \mathbf{H}_{dd} = \begin{bmatrix} 2hl^2 & 0 \\ 0 & 2hl^2 \end{bmatrix}.$$

The shear part following [13] is defined as

$$(3.16) \quad \mathbf{s}_s = \int_{h^-}^{h^+} \boldsymbol{\sigma}_s dz = \alpha_s \int_{h^-}^{h^+} \mathbf{C}_{ss} \boldsymbol{\varepsilon}_s dz = G_1 \mathbf{H}_{ss} \boldsymbol{\varepsilon}_s = G_1 \begin{bmatrix} \alpha_s h & 0 \\ 0 & \alpha_s h \end{bmatrix} \boldsymbol{\varepsilon}_s,$$

with a shear correction factor $\alpha_s = 5/6$. In the calculations α_s , l and N are assumed to be constant in the thickness direction.

We compare below the structure of elastic drilling stiffness (3.14), (3.15)₂ with form used in [13], [18–20]. For $N = (1/2)\sqrt{2}$ and $n = 0$ (the fully ceramic shell) from the equivalence condition for the elastic drilling stiffness we obtain the following identities

$$(3.17) \quad \alpha_t \frac{Eh^3}{12(1-v^2)}(1-v) = 2Ghl^2 \Leftrightarrow \alpha_t \frac{Eh^3}{12(1-v^2)}(1-v) = 2 \frac{E}{2(1+v)} hl^2$$

which yields

$$(3.18) \quad l = \sqrt{\frac{\alpha_t}{12}} h \Leftrightarrow 12 \left(\frac{l}{h} \right)^2 = \alpha_t.$$

The relation (3.18) clearly shows that α_t is a material parameter connected with the micropolar length $l = \sqrt{(1/12)\alpha_t} h$ and have not to be understood as a penalty coefficient. Hence, under given $N = (1/2)\sqrt{2}$, l and α_t have similar influence on the results.

Table 1 presents a comparison between the stress resultants components derived for functionally graded shells based on 2-D Cosserat constitutive model and for isotropic shells in 6-parameter shell theory [13]. In Table 1 we introduce for isotropic shell coefficients C and D as the tension stiffness and bending stiffness, respectively. Analogically for FGM shell: $E_1 c$ is the tension stiffness, $E_2 b$ – the coupling stiffness and $E_3 d$ – the bending stiffness. Comparing the components for FGM and isotropic shells E_1 has the sense of the effective membrane moduli, E_2 of the “coupling” moduli and E_3 of the effective bending moduli. For $n = 0$ and $n = \infty$ the resultants for FGM shells simplify to that for isotropic shells based on 2-D Cosserat constitutive model because then $E_2 = 0$ and for $n = 0$ $E_1 = E_3 = E_c$, for $n = \infty$ $E_1 = E_3 = E_m$. The stress resultants for FGM shell and isotropic shell described e.g. in [13] are equivalent, if additionally are fulfilled following conditions: $N = (1/2)\sqrt{2}$ and $l = \sqrt{(1/12)\alpha_t} h$. In FGM shells the base surface defined as geometrical medium surface is not a mechanical neutral surface because of asymmetric distribution of stiffness through the shell thickness. A consequence of that is $E_2 \neq 0$ and fact that the constitutive relations include terms coupling membrane and bending components.

Table 1. Comparison of constitutive relations for FGM and isotropic shells in 6-parameter shell theory.

Resultant	Functionally graded shell	Isotropic shell [13, 18, 19]
$N^{11} =$	$E_1c(\varepsilon_{11} + v\varepsilon_{22}) + E_2b(\kappa_{11} + \nu\kappa_{22})$	$C(\varepsilon_{11} + v\varepsilon_{22})$
$N^{22} =$	$E_1c(v\varepsilon_{11} + \varepsilon_{22}) + E_2b(\nu\kappa_{11} + \kappa_{22})$	$C(v\varepsilon_{11} + \varepsilon_{22})$
$N^{12} =$	$\frac{1-\nu}{2(1-N^2)} (E_1c[\varepsilon_{12} + (1-2N^2)\varepsilon_{21}] + E_2b[\kappa_{12} + (1-2N^2)\kappa_{21}])$	$C(1-v)\varepsilon_{12}$
$N^{21} =$	$\frac{1-\nu}{2(1-N^2)} (E_1c[(1-2N^2)\varepsilon_{12} + \varepsilon_{21}] + E_2b[(1-2N^2)\kappa_{12} + \kappa_{21}])$	$C(1-v)\varepsilon_{21}$
$Q^1 =$	$G_1\alpha_s h\varepsilon_1$	$G\alpha_s h\varepsilon_1$
$Q^2 =$	$G_1\alpha_s h\varepsilon_2$	$G\alpha_s h\varepsilon_2$
$M^{11} =$	$E_3d(\kappa_{11} + v\kappa_{22}) + E_2b(\varepsilon_{11} + v\varepsilon_{22})$	$D(\kappa_{11} + v\kappa_{22})$
$M^{22} =$	$E_3d(v\kappa_{11} + \kappa_{22}) + E_2b(v\varepsilon_{11} + \varepsilon_{22})$	$D(\kappa_{22} + v\kappa_{11})$
$M^{12} =$	$\frac{1-\nu}{2(1-N^2)} (E_3d[\kappa_{12} + (1-2N^2)\kappa_{21}] + E_2b[\varepsilon_{12} + (1-2N^2)\varepsilon_{21}])$	$D(1-v)\kappa_{12}$
$M^{21} =$	$\frac{1-\nu}{2(1-N^2)} (E_3d[(1-2N^2)\kappa_{12} + \kappa_{21}] + E_2b[(1-2N^2)\varepsilon_{12} + \varepsilon_{21}])$	$D(1-v)\kappa_{21}$
$M^1 =$	$2G_1hl^2\kappa_1$	$\alpha_t D(1-v)\kappa_1$
$M^2 =$	$2G_1hl^2\kappa_2$	$\alpha_t D(1-v)\kappa_2$
$E_1 = \frac{E_d}{n+1} + E_m, \quad E_2 = (E_c - E_m) \left[\frac{1}{(n+2)} - \frac{1}{2(n+1)} \right], \quad E_3 = (E_c - E_m) \left[\frac{3}{(n+1)} - \frac{12}{(n+2)} + \frac{12}{(n+3)} \right] + E_m,$ $G_1 = \frac{E_1}{2(1+\nu)}, \quad C = \frac{Eh}{1-\nu^2}, \quad D = \frac{Eh^3}{12(1-\nu^2)}, \quad b = \frac{h^2}{1-\nu^2}, \quad c = \frac{C}{E}, \quad d = \frac{D}{E}, \quad n \geq 0, \quad 0 < N < 1, \quad l > 0$		

4. NUMERICAL EXAMPLES

In this section we present three numerical examples which show the range of applicability of our formulation to the geometrically nonlinear analysis of smooth and irregular FGM shells. For numerical simulations we use our own FEM program written in Fortran. In numerical examples we apply the 16-node C^0 Lagrangian type shell finite element, denoted as CAMe16, with 6 DOFs at each node and fully integrated matrices. All variables from $SO(3)$ group are interpolated using the algorithm described, e.g. in [13, 22]. To increase the efficiency of calculations the solver uses the HSL library [35].

The effective moduli of FGM shells defined by equations (2.4)–(2.6) and the shell resultants depend on the volume fraction exponent n . We investigate its influence on the equilibrium paths of shell structures. However in our formulation based on 2-D Cosserat constitutive model results also depend on two micropolar constants i.e.: $N^2 = \frac{G_c}{G + G_c}$ and l . We study, therefore, the influence of coupling number and characteristic length on the arbitrary displacement for chosen load level and force for selected value of displacement or critical force.

In all examples we assume following values of Young’s modulus: $E_c = 1.51 \times 10^9$ for the ceramic constituent, $E_m = 0.7 \times 10^9$ for the metal constituent and constant value of Poisson’s ratio $\nu = 0.3$.

4.1. Annular FGM plate under end shear force

A benchmark of cut thin plate ring subjected to a distributed transverse shear force (Fig. 3) has been proposed in paper [36] as a test of shell elements

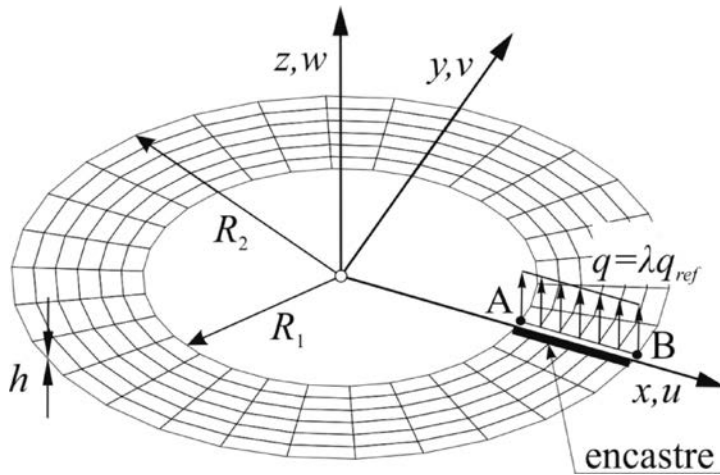


FIG. 3. Cantilever annular FGM plate strip under transverse shear force.

in the range of finite rotations. This example was considered for homogenous and isotropic plates e.g. in [13] and for functionally graded shells in [9]. The geometric quantities are given by $R_1 = 6$, $R_2 = 10$, $h = 0.03$. The analysis is performed for regular mesh 6×30 CAMe16, with 80 load steps for distributed load $q_{ref} = 0.25$. The micropolar constants are assumed as $N = \frac{\sqrt{2}}{2}$, $\frac{l}{h} = \frac{1}{1000}$. The comparison of our equilibrium curves of vertical displacement at point B for different values of power-law index n with reference solutions from paper [9] is shown in Fig. 4.

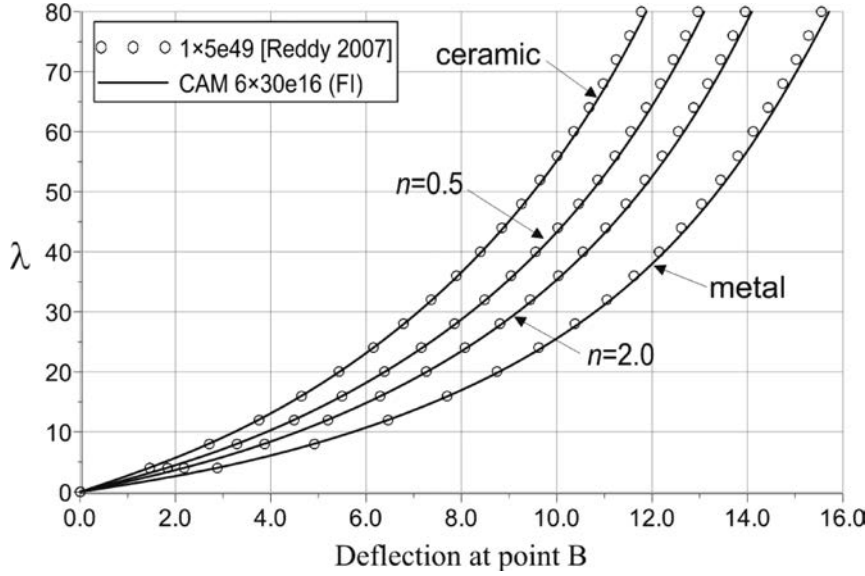


FIG. 4. Annular FGM plate strip, equilibrium curves of transverse displacement at point B for different values of n .

Then we investigate the influence of micropolar constants on normalized deflections of point B $w_{(B)}$ for load multiplier $\lambda = 80$ and $n = 0.5$. The results obtained for $N = \left\{ 0.1; \frac{\sqrt{2}}{2}; 0.9 \right\}$ and the micropolar characteristic length taken as the ratio to the shell thickness $\frac{l}{h} = \left\{ \frac{1}{1000}; \frac{1}{100}; \frac{1}{10}; 1; 10; 100 \right\}$ are compared in Fig. 5. The reference solution $w_{(B)ref} = 13.09$ is calculated for $N = \frac{\sqrt{2}}{2}$, $\frac{l}{h} = \frac{1}{1000}$.

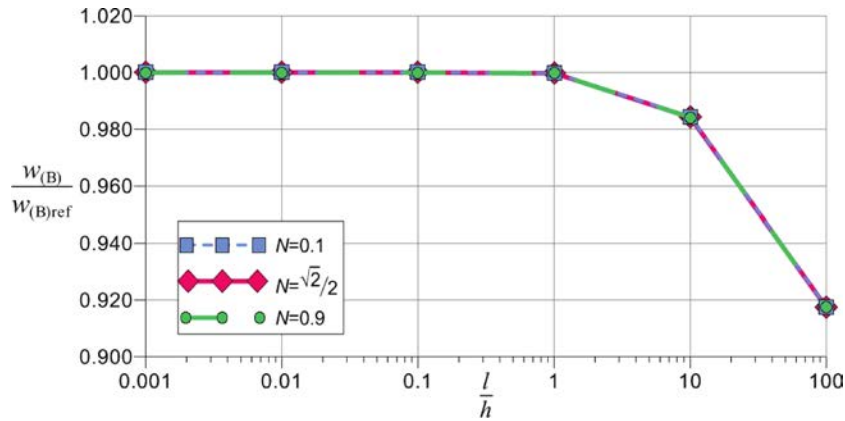


FIG. 5. Annular FGM plate strip, variable N , variable l , normalized displacement w_B for $\lambda = 80$.

4.2. Pull-out of a functionally graded cylindrical shell

As the second example we consider a functionally graded cylindrical shell with free edges (Fig. 6) which is subjected to two opposite point loads. The homogeneous case was investigated, e.g. in [13, 37] while FGM case in [9]. The following data is used in analysis: $L = 10.35$, $R = 4.953$, $h = 0.094$, $P_{ref} = 10^6$, $P = \lambda P_{ref}$. In calculations we assume that the internal surface of cylinder is made of metal and the external surface of ceramic. Due to three planes of sym-

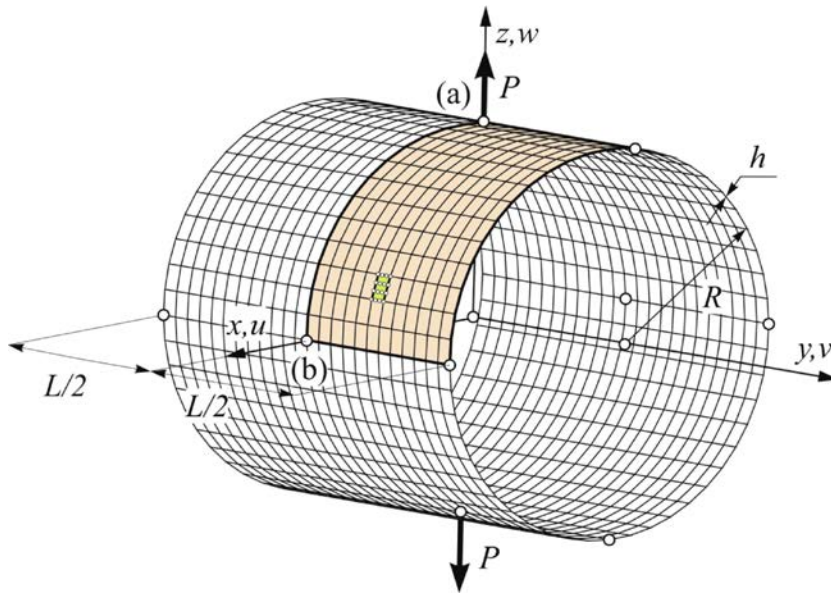


FIG. 6. Pull-out of FGM cylinder with free edges, geometry.

metry, we analyze only octant of the cylindrical shell using regular mesh 12×12 CAMe16. The micropolar constants are assumed as $N = (1/2)\sqrt{2}$ and $l = 10^{-4}$. The obtained curves of deflections at point a $w_{(a)}$ and transverse displacements at point b $u_{(b)}$ are shown in Fig. 7 and are compared to reference solutions from paper [9]. The equilibrium paths can be divided into two parts: the first being dominated by the bending stiffness and characterized by large displacements, the second is characterized by reinforcement due to increasing role of the tension stiffness. The characteristic point on the equilibrium path we call here “boundary” point.

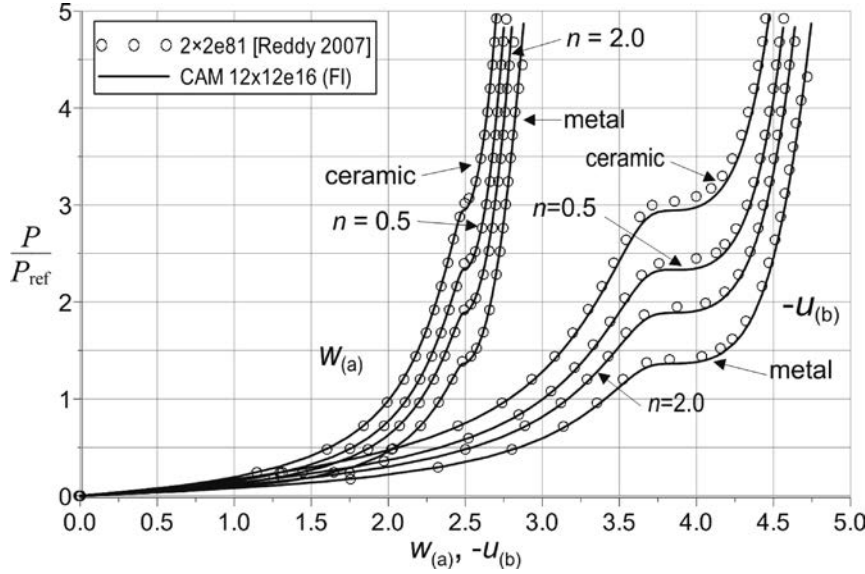


FIG. 7. Pinched FGM cylinder with free edges, equilibrium paths of radial displacements at point a and b.

Next we investigate the influence of micropolar constants on the equilibrium paths of radial displacement at point a and b. The curves calculated for $N = \left\{0.1; \frac{\sqrt{2}}{2}; 0.9\right\}$, $\frac{l}{h} = \left\{\frac{1}{1000}; 1; 10\right\}$ and $n = 2$ are depicted in Fig. 8. Then we compare in Fig. 9 values of normalized force P calculated for fixed radial displacement at point a $w_{(a)} = 2.5$ and variable micropolar parameters l and N . The value $w_{(a)} = 2.5$ responses “boundary” points on the equilibrium paths. The reference value $P_0 = 1.891$ is calculated for $N = \frac{\sqrt{2}}{2}$, $\frac{l}{h} = \frac{1}{1000}$ and the power-law index $n = 2$.

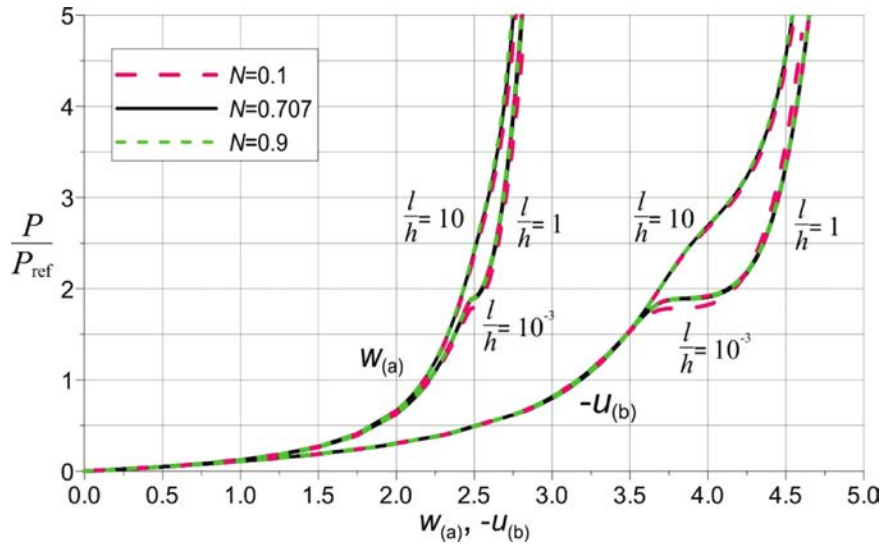


FIG. 8. Pinched FGM cylinder with free edges, influence of micropolar parameters l and N on equilibrium paths.

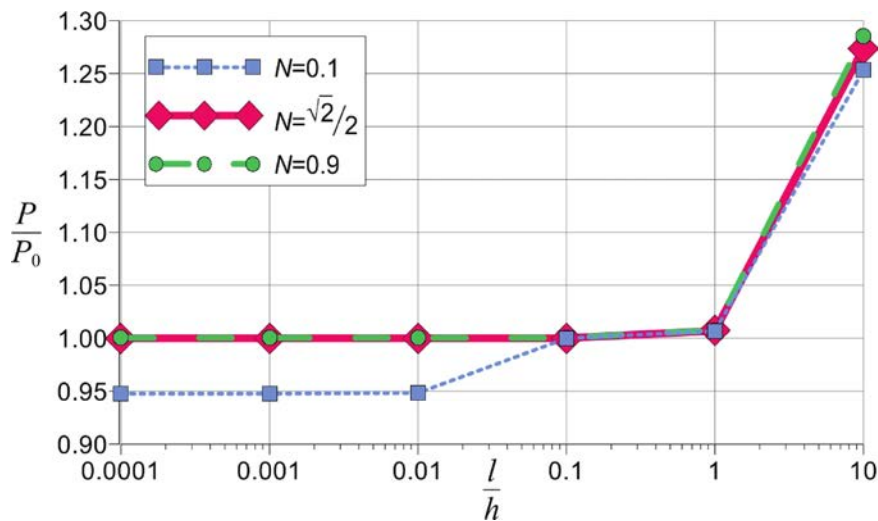


FIG. 9. Pinched FGM cylinder with free edges, variable N , variable l , normalized P for $w_{(a)} = 2.5$.

4.3. Channel section clamped beam, irregular shell

In the last numerical example we analyze a channel-section clamped beam as the example of irregular shell. The so-called drilling degree of freedom problem

makes numerical analysis of the shells with orthogonal intersections a demanding task. We wish to emphasize that in our formulation based on the 6-parameter shell theory the drilling DOF is naturally defined, so this issue is absent. The geometry of the cantilever channel-section beam loaded with vertical force at the free end is presented in Fig. 10. This example was described originally in [18] for purely elastic homogenous shell and later studied, e.g. in [13, 21]. The results for elastoplastic analysis are presented, for instance in [23, 24, 38]. For large displacement and rotation analysis the solution of this example has mainly shell character, therefore in calculations we use shell model instead of the beam theory.

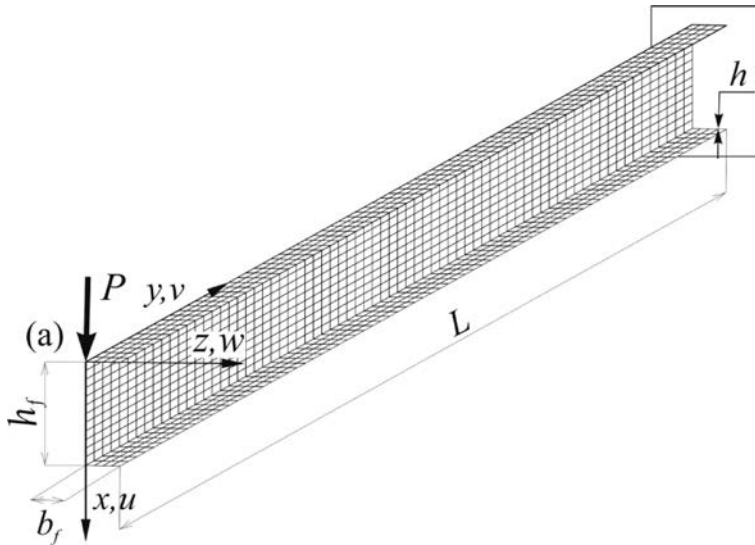


FIG. 10. Geometry of the channel section clamped beam.

The following data is used in analysis: $L = 36$, $h_f = 6$, $b_f = 2$, $h = 0.05$, $P_{\text{ref}} = 10000$, $P = \lambda P_{\text{ref}}$. We assume that internal surfaces of channel section beam are made of metal and external surfaces of ceramic. For computation the regular discretization $(4 + 8 + 4) \times 36$ CAME16, i.e. number of elements per: (flange+web+flange) \times length, is chosen. The following values of the micropolar constants are used: $N = (1/2)\sqrt{2}$ and $l = 10^{-4}$. Figure 11 shows the comparison of our results with solutions calculated in commercial program Abaqus, as there is not available in literature any reference solution for FGM channel section beam. In Abaqus we model FGM shell as composite shell consisting of 10 layers using the simplified method described at the end of the Sec. 2. In calculations we used the discretization $(4 + 6 + 4) \times 36$ of eight node elements with reduced integration of matrices S8R. The influence of the power-law index

n on equilibrium paths is depicted in Fig. 11. In Table 2 for different values of n are compared values of load multiplier for curve limit points.

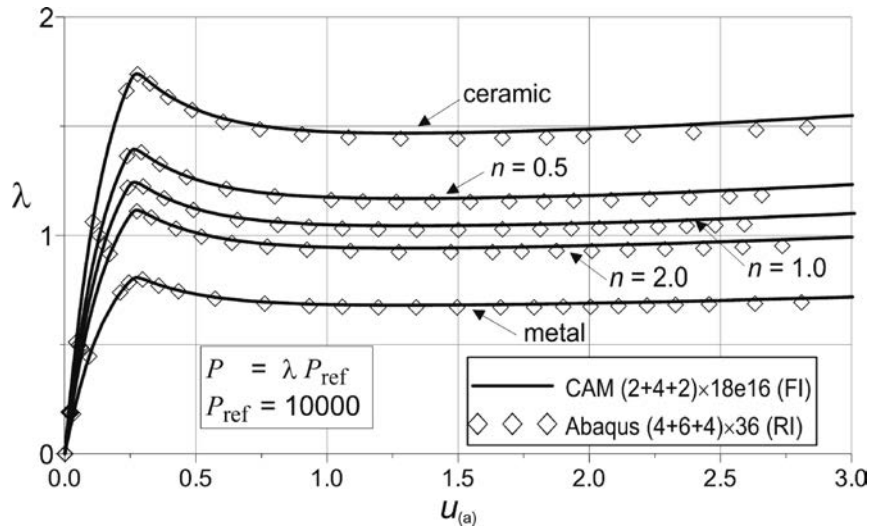


FIG. 11. Channel section clamped beam, equilibrium paths of deflection $u_{(a)}$ for different values of exponent n .

Table 2. The influence of exponent n on loci of the limit point for the channel section.

Power-law index n	Load multiplier λ
0	1.741
0.5	1.394
1	1.244
2	1.115
10^6	0.807

Next we investigate the influence of the micropolar parameter N and ratio l/h on value of P for the limit point. The results calculated for $N = \left\{ 0.1; \frac{\sqrt{2}}{2}; 0.9 \right\}$ and ratio $\frac{l}{h} = \left\{ \frac{1}{1000}; \frac{1}{100}; \frac{1}{10}; 1; 10 \right\}$ are compared in Fig. 12. The reference solution $P_0 = 1.115$ is obtained for $N = \frac{\sqrt{2}}{2}$, $\frac{l}{h} = \frac{1}{1000}$ and exponent $n = 2$.

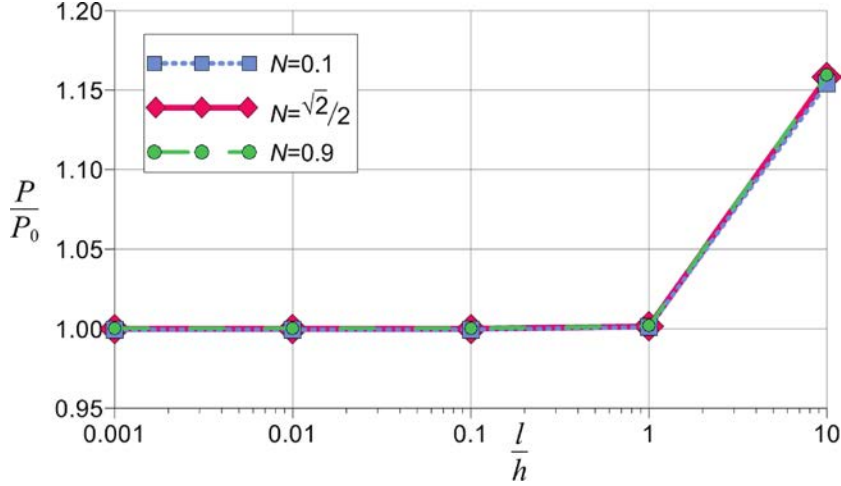


FIG. 12. Channel section clamped beam, variable N , variable l , normalized P for limit point.

5. CONCLUSIONS

In this paper, we have presented the formulation based on 2-D Cosserat constitutive model appropriate for the resultant 6-parameter shell theory. We used this formulation to derive the elastic constitutive relation for functionally graded shells. We assumed that FGM shell is made of two isotropic constituents: ceramic and metal and the variation of properties through the thickness is defined by the power law. The geometrically nonlinear analysis have been performed for two examples of the regular FGM shells: annular plate strip and pinched cylinder with free edges. The calculated equilibrium paths show very good agreement with the reference solutions from paper [9]. Additionally our formulation allows for correct analysis of irregular shells, therefore in this paper we extended the set of reference solutions available in literature for functionally graded shells with the example of FGM channel section clamped beam. The numerical results of geometrically nonlinear analysis show that

- response curves of FGM shells under mechanical loading lie between curves of ceramic and metal shells and has similar character like response curves of homogenous shells;
- power-law index n has a big influence on the results.

The simplified method for modelling of FGM shell as composite shell consisting of many layers, used in the commercial program Abaqus, gives the results in good agreement with that obtained by the exact formulation.

The Cosserat constitutive relation used in our formulation has two additional material parameters, i.e. the micropolar parameter N and the micropolar

characteristic length l . The numerical results obtained for thin shells show that parameter N has very small influence on the results, noticeable only in the example of pinched FGM cylinder with free edges. The common conclusion for all examples is that for $l/h < \sim 1$ the equilibrium curves do not show significant discrepancies. However, values of $l/h > \sim 1$ cause stiffening effect and in some examples have qualitative influence on the results. So to avoid discrepancies between our formulation and the reference solutions we propose the range of l/h should be from 0 to 1. The influence of ratio l/h on shell behaviour obtained in this work for FGM shell is similar to that presented for homogenous shells, for instance in [23, 24, 30].

ACKNOWLEDGMENT

Parallel solver for CAM elements is developed on the basis of HSL [35], a collection of Fortran codes for large-scale scientific computation,

<http://www.hsl.rl.ac.uk>

The ABAQUS calculations presented in this paper were carried out at the TASK, Academic Computer Center in Gdansk, Poland.

Karol Daszkiewicz is supported by grants from Faculty of Civil and Environmental Engineering, Gdańsk University of Technology.

REFERENCES

1. KOIZUMI M., *FGM activities in Japan*, Composites Part B, **28B**, 1–4, 1997, <http://www.sciencedirect.com/science/article/pii/S1359836896000169>.
2. KREJA I., *A literature review on computational models for laminated composite and sandwich panels*, Central European Journal of Engineering, **1**, 59–80, 2011, <http://link.springer.com/article/10.2478%2Fs13531-011-0005-x>.
3. WOO J., MEGUID S.A., *Nonlinear analysis of functionally graded plates and shallow shells*, International Journal of Solids and Structures, **38**, 7409–7421, 2001, <http://www.sciencedirect.com/science/article/pii/S0020768301000488>.
4. GHANNADPOUR S.A.M., ALINIA M.M., *Large deflection behavior of functionally graded plates under pressure loads*, Composite Structures, **75**, 67–71, 2006, <http://www.sciencedirect.com/science/article/pii/S0263822306001188>.
5. CHI S., CHUNG Y., *Mechanical behavior of functionally graded material plates under transverse load – Part I: Analysis*, International Journal of Solids and Structures, **43**, 3657–3674, 2006, <http://www.sciencedirect.com/science/article/pii/S0020768305002052>.
6. CHI S., CHUNG Y., *Mechanical behavior of functionally graded material plates under transverse load – Part II: Numerical results*, International Journal of Solids and Structures, **43**, 3675–3691, 2006, <http://www.sciencedirect.com/science/article/pii/S0020768305002040>.

7. YANG J., SHEN H.-S., *Non-linear analysis of functionally graded plates under transverse and in-plane loads*, International Journal of Nonlinear Mechanics, **38**, 467–482, 2003, <http://www.sciencedirect.com/science/article/pii/S0020746201000701>.
8. MA L.S., WANG T.J., *Nonlinear bending and postbuckling of functionally graded circular plates under mechanical and thermal loadings*, International Journal of Nonlinear Mechanics, **40**, 3311–3330, 2003, <http://www.sciencedirect.com/science/article/pii/S0020768303001185>.
9. ARCINIEGA R.A., REDDY J.N., *Large deformation analysis of functionally graded shells*, International Journal of Solids and Structures, **44**, 2036–2052, 2007, <http://www.sciencedirect.com/science/article/pii/S0020768306003428>.
10. SHEN H.-S., *Functionally Graded Materials, Nonlinear Analysis of Plates and Shells*, CRC Press, Boca Raton, London, New York, 2009.
11. MANIA R.J., *Dynamic response of FGM thin plate subjected to combined loads*, [in:] *Shell Structures: Theory and Applications*, Vol. 3, 377–380, W. Pietraszkiewicz and J. Górski [Eds.], CRC Press, London, 2014.
12. ZHANG D.-G., *Nonlinear bending analysis of FGM rectangular plates with various supported boundaries resting on two-parameter elastic foundations*, Archive of Applied Mechanics, **84**, 1, 1–20, 2014, <http://link.springer.com/article/10.1007%2Fs00419-013-0775-0>.
13. CHRÓŚCIELEWSKI J., MAKOWSKI J., PIETRASZKIEWICZ W., *Statyka i Dynamika Powłok Wielopłatowych, Statics and dynamics of multifold shells: Nonlinear theory and finite element method* (in Polish), Wydawnictwo IPPT PAN, Warsaw, 2004.
14. COSSERAT E., COSSERAT F., *Théorie des corps déformables, Theory of deformable bodies* (in French), Librairie Scientifique A. Hermann et Fils, Paris, 1909.
15. NOWACKI W., *Theory of asymmetric elasticity*, Pergamon Press, Oxford, 1986.
16. RUBIN M.B., *Cosserat Theories: Shells, Rods and Points*, Kluwer Academic Publishers, Dordrecht, 2000.
17. ALTENBACH J., ALTENBACH H., EREMEYEV V.A., *On generalized Cosserat-type theories of plates and shells: a short review and bibliography*, Archive of Applied Mechanics, **80**, 73–92, 2010, <https://hal.archives-ouvertes.fr/hal-00827365>.
18. CHRÓŚCIELEWSKI J., MAKOWSKI J., STUMPF H., *Genuinely resultant shell finite elements accounting for geometric and material non-linearity*, Int. J. Numer. Meth. Eng., **35**, 63–94, 1992, <http://onlinelibrary.wiley.com/doi/10.1002/nme.1620350105/abstract>.
19. CHRÓŚCIELEWSKI J., WITKOWSKI W., *4-node semi-EAS element in 6-field nonlinear theory of shells*, International Journal for Numerical Methods in Engineering, **68**, 1137–1179, 2006, <http://onlinelibrary.wiley.com/doi/10.1002/nme.1740/abstract>.
20. KONOPÍŃSKA W., PIETRASZKIEWICZ W., *Exact resultant equilibrium conditions in the non-linear theory of branching and self-intersecting shells*, International Journal of Solids and Structures, **44**, 352–369, 2007, <http://www.sciencedirect.com/science/article/pii/S0020768306001405>.
21. WIŚNIEWSKI K., *Finite rotation shells: Basic equations and finite elements for Reissner kinematics*, Springer, Berlin, 2010, <http://link.springer.com/book/10.1007%2F978-90-481-8761-4>.

22. CHRÓSCIELEWSKI J., KREJA I., SABIK A., WITKOWSKI W., *Modeling of composite shells in 6-parameter nonlinear theory with drilling degree of freedom*, Mech. Adv. Mater. Struct., **18**, 403–419, 2011, <http://www.tandfonline.com/doi/abs/10.1080/15376494.2010.524972#.U7SDhrE09I0>.
23. BURZYŃSKI S., CHRÓSCIELEWSKI J., WITKOWSKI W., *Elastoplastic material law in 6-parameter nonlinear shell theory*, [in:] *Shell Structures: Theory and Applications*, Vol. 3, 377–380, W. Pietraszkiewicz and J. Górski [Eds.], CRC Press, London, 2014.
24. BURZYŃSKI S., CHRÓSCIELEWSKI J., WITKOWSKI W., *Elastoplastic law of Cosserat type in shell theory with drilling rotation*, Mathematics and Mechanics of Solids, DOI: 10.1177/1081286514554351, <http://mms.sagepub.com/content/early/2014/10/16/1081286514554351>.
25. DASZKIEWICZ K., *Nonlinear analysis of functionally graded shells in micropolar elasticity* [in Polish: *Analiza nieliniowa powłok z materiałów gradientowych w ośrodku mikropolarnym*], [in:] *Wiedza i eksperymenty w budownictwie*, J. Bzówka [Ed.], Wydawnictwo Politechniki Śląskiej, Gliwice, 765–772, 2014.
26. DASZKIEWICZ K., CHRÓSCIELEWSKI J., WITKOWSKI W., *The influence of micropolar material constants on MES geometrically nonlinear analysis of FGM shells* [in Polish: *Wpływ parametrów materiałowych ośrodka mikropolarnego na geometrycznie nieliniową analizę MES powłok z materiałów o funkcyjnej gradacji właściwości materiałowych*], [in:] XIII Konferencja Naukowo-Techniczna TKI 2014, Techniki Komputerowe w Inżynierii, Abstracts, Wydawnictwo WAT, Warszawa, 45–46, 2014.
27. REDDY J.N., *Mechanics of Laminated Composite Plates and Shells: Theory and Analysis*, CRC Press, Boca Raton, London, New York, Washington D.C., 2003.
28. KUGLER S., FOTIU P.A., MURIN J., *The numerical analysis of FGM shells with enhanced finite elements*, Engineering Structures, **49**, 920–935, 2013, <http://www.sciencedirect.com/science/article/pii/S0141029613000035>.
29. PIETRASZKIEWICZ W., BADUR J., *Finite rotations in the description of continuum deformation*, International Journal of Engineering Science, **21**, 1097–1115, 1983, <http://www.sciencedirect.com/science/article/pii/0020722583900502>.
30. JEONG J., RAMEZANI H., MÜNCH I., NEFF P., *A numerical study for linear isotropic Cosserat elasticity with conformally invariant curvature*, Z. Angew. Math. Mech., **89**, 7, 552–569, 2009, <http://onlinelibrary.wiley.com/doi/10.1002/zamm.200800218/abstract>.
31. LAKES R.S., *Experimental microelasticity of two porous solids*, International Journal of Solids Structures, **22**, 1, 55–63, 1986, <http://www.sciencedirect.com/science/article/pii/0020768386901034>.
32. LAKES R.S., *Experimental methods for study of Cosserat elastic solids and other generalized elastic continua*, [in:] *Continuum models for materials with micro-structure*, 1–22, Mhlhaus H. [Eds.], Wiley, 1995, <http://silver.neep.wisc.edu/~lakes/CossRv.pdf>.
33. KHABBAZ R.S., MANSHADI B.D., ABEDIAN A., *Nonlinear analysis of FGM plates under pressure loads using higher-order shear deformation theories*, Composite Structures, **89**, 333–344, 2009, <http://www.sciencedirect.com/science/article/pii/S0263822308002055>.
34. PIETRASZKIEWICZ W., KONOPIŃSKA V., *Drilling couples and refined constitutive equations in the resultant geometrically non-linear theory of elastic shells*, International Journal of Solids Structures, **51**, 11–12, 2133–2143, 2014, <http://www.sciencedirect.com/science/article/pii/S0020768314000705>.

35. HSL, *A collection of Fortran codes for large-scale scientific computation*, <http://www.hsl.rl.ac.uk/>.
36. BASAR Y., DING Y., *Finite rotation elements for the nonlinear analysis of thin shell structures*, *International Journal of Solids and Structures*, **26**, 83–97, 1990, <http://www.sciencedirect.com/science/article/pii/002076839090096E>.
37. SANSOUR C., BEDNARCZYK H., *The Cosserat surface as a shell model, theory and finite-element formulation*, *Computational Methods in Applied Mechanics and Engineering*, **120**, 1–32, 1995, <http://www.sciencedirect.com/science/article/pii/004578259400054Q#>.
38. EBERLEIN R., WRIGGERS P., *Finite element concepts for finite elastoplastic strains and isotropic stress response in shells: theoretical and computational analysis*, *Computer Methods in Applied Mechanics and Engineering*, **171**, 243–279, 1999, <http://www.sciencedirect.com/science/article/pii/S0045782598002126>.

Received July 3, 2014; revised version October 8, 2014.
